Pauli rearrangement potential for a scattering state with the nucleon-nucleon interaction in chiral effective field theory

M. Kohno (河野通郎)*
Research Center for Nuclear Physics, Osaka University, Ibaraki 567-0047, Japan

(Received 24 August 2018; published 28 November 2018)

The Pauli rearrangement potential given by the second-order diagram is evaluated for a nucleon optical model potential (OMP) with G matrices of the nucleon-nucleon interaction in chiral effective field theory. The results obtained in nuclear matter are applied for ^{40}Ca in a local-density approximation. The repulsive effect is of the order of 5–10 MeV at the normal density. The density dependence indicates that the real part of the microscopic OMP becomes shallower in a central region, but is barely affected in a surface area. This improves the overall resemblance of the microscopic OMP to the empirical one.

DOI: 10.1103/PhysRevC.98.054617

I. INTRODUCTION

An optical model potential (OMP) embodies a basic character of describing the nucleon elastic scattering on nuclei. The success of the global parametrization of the phenomenological OMP with certain geometric parameters and a moderately energy-dependent strength suggests that a mean field picture holds for scattering states as for bound nucleons. The OMP consists of the real and imaginary components. The former is regarded as a mean field similar to a single-particle (s.p.) potential of the ground state, as a consequence of the interaction between the incoming nucleon and the nucleons in a target nucleus. The imaginary part takes care of the escaping of an incident flux to inelastic channels.

Microscopic understanding and an explicit evaluation of the OMP, starting from bare nucleon-nucleon (*NN*) interactions, have been one of the basic problems in nuclear physics. Jeukenne, Lejeune, and Mahaux [1–3] developed a nuclear matter approach. The properties of the s.p. potential evaluated in nuclear matter were discussed and a local-density approximation was used for finite nuclei. Brieva and Rook [4,5] offered a somewhat different method. A density- and energy-dependent complex effective *NN* interaction was prepared based on G matrices in nuclear matter and was applied to construct a folding potential for finite nuclei, using their localization method of exchange terms. This study is the prototype of the subsequent G-matrix folding model of the microscopic OMP.

Recent microscopic calculations by several groups [6–8] with various realistic *NN* forces are remarkably successful in accounting for nucleon-nucleus scattering data. The OMP by Amos *et al.* [6], the Melbourne group, with the Paris [9] or Bonn-B [10] potentials worked well, in spite of the fact that those interactions fail to reproduce proper nuclear saturation properties. This implies that the description of nucleon-nucleus scattering is not sensitive to the saturation properties. Nevertheless, it is appropriate to employ the framework in which the saturation properties are realized. Furumoto *et al.* [7] were concerned with the saturation properties by adding the effects of phenomenological three-nucleon forces (3NFs) to the Nijmegen extended soft-core *NN* potential [11,12]. The Kyushu group [8] employed the next-to-next-to-next-to-leading (N^{3}LO) interaction in chiral effective field theory (ChEFT) [13] with including the effect of the next-to-next-to-leading (N^{2}LO) 3NFs [14] in the normal-ordering prescription [15]. These calculations remain in the lowest-order in the Brueckner expansion for the OMP. The next-order contribution was discussed in the early stage of microscopic studies [2]. It was recognized that the contribution of the second-order rearrangement process becomes smaller with increasing the incident energy, and therefore the actual incorporation of this contribution has been left out in the recent microscopic OMPs [6–8]. For a deeper understanding of the microscopic OMP, however, it is worthwhile to revisit the issue of the Pauli rearrangement for the OMP.

The concept of the rearrangement energy was presented by Brueckner and Goldman [16] in the development of the Brueckner theory [17]. Its important role stems from the strong correlations with the *NN* forces having short-range singularities and Pauli blocking effects. The rearrangement potential plays a decisive role to reproduce ground state properties of nuclei, which has been popularized as the potential generated through the derivative of the density-dependent terms of effective *NN* interactions in a density-dependent Hartree-Fock description of nuclei. The density dependence originates partly from the Pauli effects in the Brueckner theory. Another source of the density dependence is the contribution of the 3NFs. The main effect of the 3NFs itself can be regarded as the rearrangement effect due to the Pauli principle acting in the process which includes the excitation of non-nucleonic degrees of freedom [15].

In the present article, the contribution of the second-order Pauli rearrangement diagram for a nucleon scattering state is calculated first in symmetric nuclear matter and then its implication in finite nuclei is discussed in a local-density approximation. The treatment is intended to extend the microscopic

*kohno@rcnp.osaka-u.ac.jp

derivation of the OMP [8,18,19] starting with the *NN* and 3NF forces parametrized in ChEFT [13,14]. As is shown in this article, the inclusion of the Pauli rearrangement potential improves the correspondence between the microscopic OMP and the empirical one.

Holt *et al.* [20] reported a microscopic calculation of the OMP in symmetric nuclear matter, at second order in perturbation theory. Their choice of ChEFT N^3LO *NN* and N^2LO 3NF interactions with the cutoff scale of $\Lambda \simeq 2.5$ fm^{-1} allows the use of the perturbative framework. The G-matrix calculation in the present article should give quantitatively similar results to theirs. Here, the results with the larger cutoff scale are also shown.

In Sec. II, basic expressions are given to the Pauli rearrangement potential in the second order. Numerical results in symmetric nuclear matter using ChEFT interactions are presented in Sec. III A. The implication of the result in finite nuclei is discussed in Sec. III B, using a simple local-density approximation. The conclusions follow in Sec. IV.

II. REARRANGEMENT POTENTIAL

Ladder correlation is essential for the *NN* interaction in nuclei to regularize short-range singularities of the bare *NN* force. The correlation naturally depends on the nuclear structure through Pauli effects and the change of the nucleon propagator. The G-matrix equation in the framework of the Brueckner theory [17] properly takes care of these effects, which is written as

$$G(\omega)|ij\rangle = v|ij\rangle + v\frac{Q}{\omega - H_0}G(\omega)|ij\rangle, \tag{1}$$

where v is a bare *NN* force, $|ij\rangle$ specifies a two-nucleon state, ω is a sum of s.p. energies $\omega = e_i + e_j$, and the Hamiltonian H_0 is given by the sum of the kinetic energies and the nucleon s.p. potentials, $H_0 = t_i + U_i + t_j + U_j$. Once the short-range repulsive part is regularized, the resulting interaction, the G matrix, qualifies for a mean-field description of low energy nuclear properties. The interaction between an incoming nucleon and a nucleon in a target nucleus is also considered in the similar framework.

The microscopic OMP is assigned in the lowest order to the folding potential of the G matrices with respect to the target wave functions. The method commonly used [5] is to prepare density- and energy-dependent complex effective interactions on the basis of nuclear matter calculations, and to apply them in the folding procedure to finite nuclei.

The next-order contribution, the second-order process in terms of the G matrix, is shown in Fig. 1(a). This arises as Pauli blocking of the ground state energy of the target nucleus due to the incoming nucleon, Fig. 1(b). The degree of the importance of this Pauli blocking effect reflects the importance of the ladder correlation in the ground state. Taking spin and isospin average for the particle state $\boldsymbol{p}$, the rearrangement potential from the diagram Fig. 1(a) is evaluated as

$$U_{\rm rear}(\boldsymbol{p}) = -\frac{1}{8}\sum_{\sigma_p,\tau_p}\sum_{\sigma_{p'},\tau_{p'}}\sum_{\sigma_{h'},\tau_{h'}}\sum_{\sigma_h,\tau_h}\sum_{\boldsymbol{p}'}\sum_{\boldsymbol{h},\boldsymbol{h}'} \times \frac{|\langle \boldsymbol{p}\boldsymbol{p}'|G|\boldsymbol{h}\boldsymbol{h}'\rangle_A|^2}{e_{\boldsymbol{h}} + e_{\boldsymbol{h}'} - e_{\boldsymbol{p}} - e_{\boldsymbol{p}'}}, \tag{2}$$

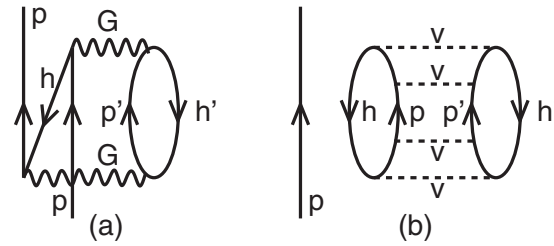

FIG. 1. (a) Pauli rearrangement diagram in the second order. (b) Illustration of the Pauli blocking in a ground-state ladder correlation.

where $\boldsymbol{h}$ and $\boldsymbol{h}'$ stand for occupied states (in nuclear matter $|\boldsymbol{h}| \leqslant k_F$ and $|\boldsymbol{h}'| \leqslant k_F$ with k_F being the Fermi momentum) and $\boldsymbol{p}'$ represents an unoccupied state (in nuclear matter $|\boldsymbol{p}'| > k_F$). The suffix A of the matrix element denotes antisymmetrization. The summation over $\boldsymbol{p}'$ is redundant because of the momentum conservation $\boldsymbol{p} + \boldsymbol{p}' = \boldsymbol{h} + \boldsymbol{h}'$. The potential $U_{\rm rear}(\boldsymbol{p})$ is apparently real and positive. Partial wave expansion is introduced in evaluating G matrices in nuclear matter, and an angle average is commonly used for the Pauli operator Q and the propagator in Eq. (1). The angle average is also used in the present calculation of Eq. (2). If the G matrices are parametrized as a local interaction in a functional form, such as Gaussian, the partial wave expansion is not necessary. The comparison of the calculations with and without the angle average for such a parameterized effective interaction shows that the angle average works very well.

As the Pauli effect, the rearrangement potential is similar to the contribution of 3NFs, e.g., the process including Δ-isobar excitation typically. The excitation of non-nucleonic degrees of freedom that is usually implicit in the *NN* potential should be Pauli-blocked in the nuclear medium, Fig. 2(a). Repulsive effects of this suppression plays an important role to quantitatively reproduce nuclear saturation properties [15]. The contributions of the 3NFs for describing nucleon-nucleus and nucleus-nucleus scattering problems have been discussed in recent years [8], using the N^2LO 3NFs in ChEFT. The process is illustrated in Fig. 2(b). However, the estimation of the analogous contributions of the diagram of Fig. 1(a) has not been considered. The comparison between the contributions of Figs. 1(a) and 2(b) is discussed in Sec. III B.

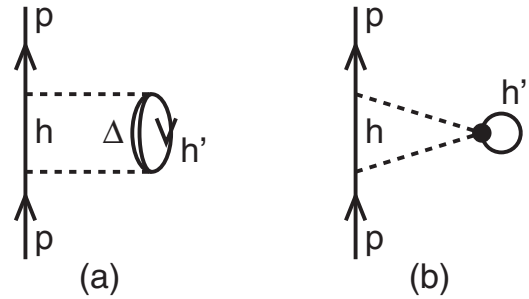

FIG. 2. Example of the Pauli blocking process of the 2π exchange 3BF: (a) Fujita-Miyazawa type and (b) ChEFT contact term.

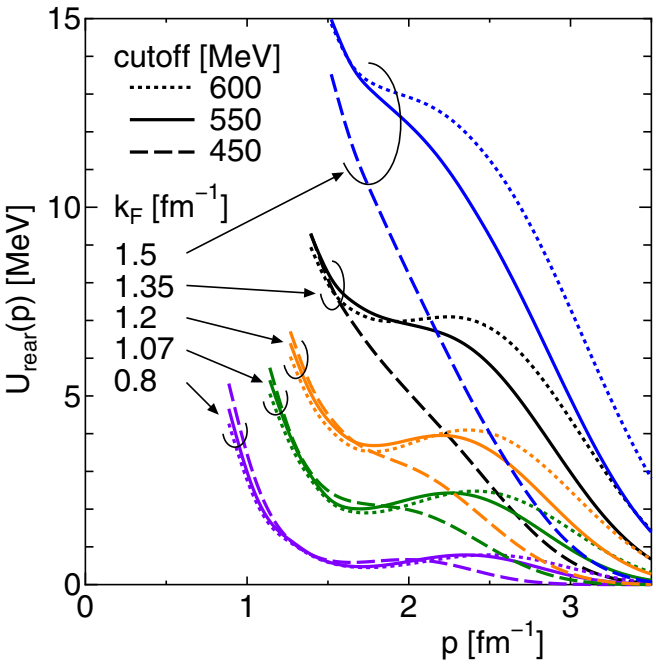

FIG. 3. Momentum dependence of the Pauli rearrangement potential in symmetric nuclear matter with various Fermi momenta from 0.8 to 1.5 fm^{-1}. ChEFT interactions [13] including 3NF effects are employed with three different cutoff scales: 450, 550, and 600 MeV, respectively.

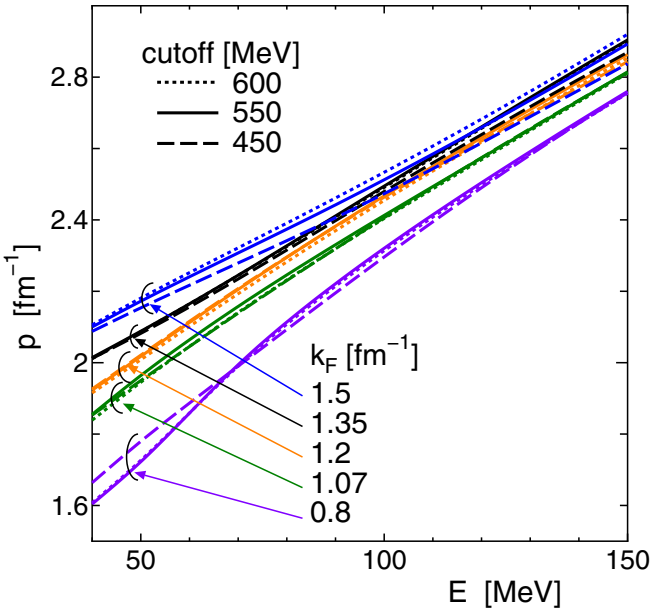

FIG. 4. Relation between the energy E and the momentum p in symmetric nuclear matter specified by Eq. (3).

III. NUMERICAL RESULTS

A. Results in nuclear matter

The *NN* interaction in ChEFT parametrized by Epelbaum *et al.* [13] is used as the bare force. The effects of 3NFs [14] are included in a normal-ordering prescription. The G-matrix calculations in nuclear matter in the lowest-order Brueckner theory are reported in Ref. [15], in which the parameters of the contact 3NFs, c_D and c_E, are adjusted so as to reproduce reasonably well nuclear matter saturation properties. The application of these G matrices to describing nucleon-nucleus and nucleus-nucleus scattering processes is presented in Refs. [8,19].

Figure 3 shows calculated results of the Pauli rearrangement potential in symmetric nuclear matter as a function of the nucleon momentum p for five cases of the Fermi momentum; 0.8, 1.07, 1.2, 1.35, and 1.5 fm^{-1} which correspond to the nucleon density as $0.21\rho_0$, $0.5\rho_0$, $0.70\rho_0$, ρ_0, and $1.37\rho_0$, respectively, with the normal density being $\rho_0 = \frac{2}{3\pi^2}(1.35)^3 = 0.166$ fm^{-3}.

The Pauli rearrangement potential decreases fast as the momentum p increases. Instead of the momentum p, the s.p. energy E of the nucleon is more adequate to specify the nucleon state in the nuclear medium to describe nucleon-nucleus scattering, which is related to the momentum p by the relation including a s.p. potential $U_{\rm LO}(p, k_F)$:

$$E = \frac{\hbar^2}{2m}p^2 + U_{\rm LO}(p, k_F), \tag{3}$$

where the suffix LO means the lowest-order s.p. potential in nuclear matter. As explained in Ref. [15], the following prescription is adopted for $U_{\rm LO}(p)$ when the effective two-body interactions $V_{12(3)}$ deduced from 3NFs by a normal-ordering prescription are incorporated:

$$U_{\rm LO}(p, k_F) = \sum_{|\boldsymbol{p}'|\leqslant k_F} \langle \boldsymbol{p}\boldsymbol{p}'|G + \frac{1}{6}V_{12(3)}\left(1 + \frac{Q}{\omega - H}\right)G|\boldsymbol{p}\boldsymbol{p}'\rangle_A. \tag{4}$$

The relation between p and E in nuclear matter with the present ChEFT interaction is shown in Fig. 4. The Pauli rearrangement potential as a function of the energy E is presented in Fig. 5. The energy dependence is gentle. Though some cutoff scale dependence is seen, the strength is not negligible as far as the density is larger than half the normal density.

It is instructive to carry out similar calculations with other modern *NN* interactions; AV18 [21], NSC97 [22], and CD-Bonn [23] potentials. Results are shown in Fig. 6. The AV18 potential provides the largest rearrangement potential among them, the strength of which is comparable to that of the ChEFT interactions with the cutoff scale of $\Lambda = 550$ and 600 MeV.

B. Optical model potential in ^{40}Ca

It is worthwhile to consider the rearrangement potential in finite nuclei. Because the rearrangement potential obtained in nuclear matter is a one-body quantity, it does not apply in a standard procedure of constructing a folding potential of effective two-body interactions. In order to estimate the contribution of the rearrangement potential in a finite nucleus

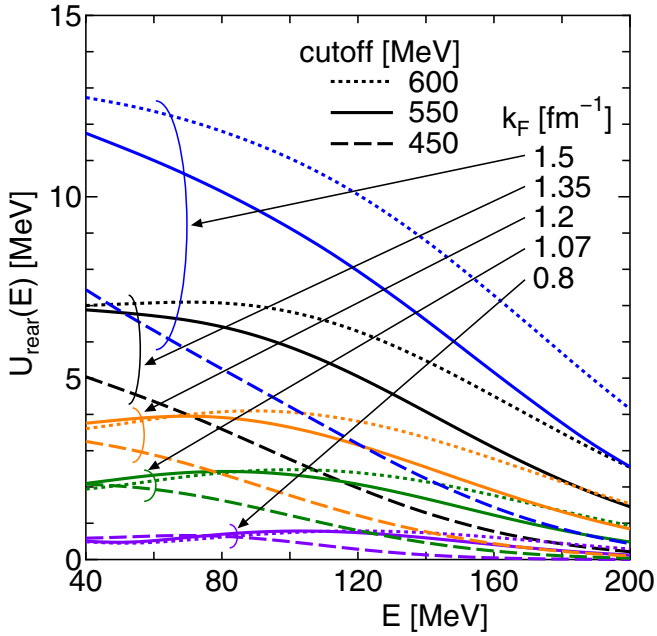

FIG. 5. Energy dependence of the Pauli rearrangement potential in symmetric nuclear matter with various Fermi momenta from 0.8 to 1.5 fm^{-1}. ChEFT interactions [13] including 3NF effects are employed with three different cutoff scales: 450, 550, and 600 MeV, respectively.

from the result of the nuclear matter calculation, a simple local-density approximation is employed.

In symmetric nuclear matter, the nucleon density ρ is related to the Fermi momentum k_F as $\rho = \frac{2}{3\pi^2}k_F^3$. A naive

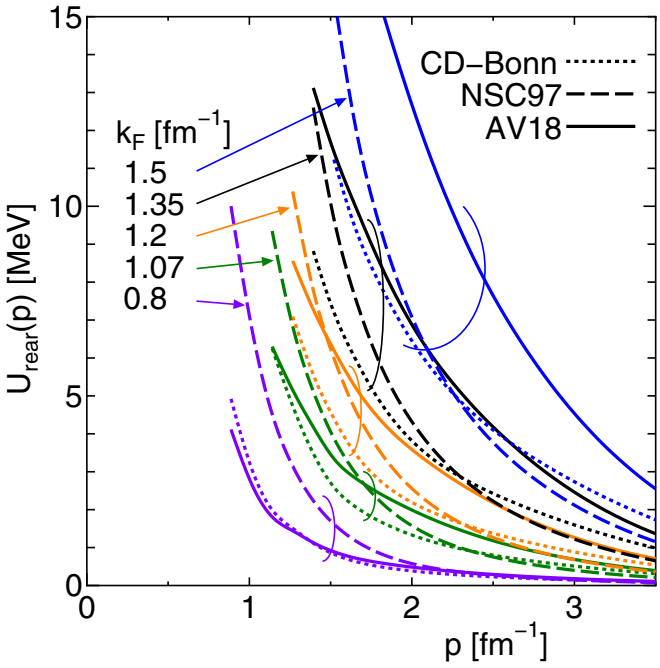

FIG. 6. Momentum dependence of the Pauli rearrangement potential in symmetric nuclear matter calculated with AV18 [21], NSC97 [22], and CD-Bonn [23] *NN* potentials.

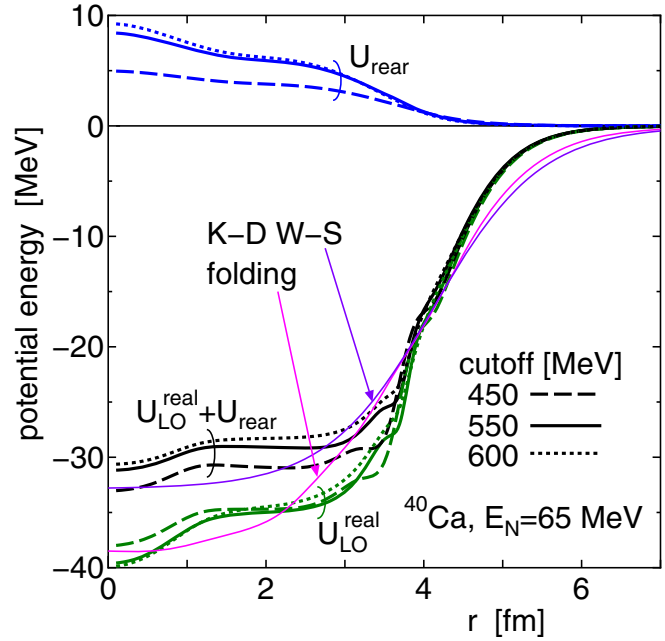

FIG. 7. Radial dependence of the real part of the optical model potential for the nucleon incident energy $E_N = 65$ MeV evaluated by a simple local-density approximation prescription for ^{40}Ca. The lowest-order potential $U_{\rm LO}^{\rm real}$, Pauli rearrangement potential $U_{\rm rear.}$, and the sum of them are plotted for three cases of the cutoff scale of the ChEFT interactions. The thin solid curve labeled "folding" represents a localized folding potential [25] obtained with the density-dependent effective two-body interaction parametrized on the basis of G matrices in nuclear matter [8]. The thin solid curve labeled "K-D W-S" is a Woods-Saxon potential by Koning and Delaroche [26].

prescription to obtain a potential in a finite nucleus suggested by the potential $U(p, k_F)$ calculated in nuclear matter is to replace the Fermi momentum k_F by a local quantity of $(3\pi^2\rho(r)/2)^{1/3}$. The momentum p is connected with the incident energy E by solving Eq. (3).

The results for ^{40}Ca obtained in this prescription are shown in Figs. 7 and 8 for the incident energy of 65 MeV and 100 MeV, respectively. The density distribution of ^{40}Ca is provided by Hartree-Fock wave functions with the Gogny D1S effective force [24]. The curves marked by $U_{\rm LO}^{\rm real}$ in these figures represent the lowest-order potential before incorporating the Pauli rearrangement contribution. It is noteworthy that the shape and the strength of this $U_{\rm LO}^{\rm real}$ corresponds well to that of the folding potential [25] calculated with the density-dependent effective two-body interaction parametrized on the basis of G matrices of ChEFT interactions [8] which is shown by a thin solid curve labeled "folding", although the surface thickness is smaller because of the lack of finite-range effects in the local-density approximation. This good correspondence assures the usefulness of the local-density approximation for estimating the contribution of the Pauli rearrangement effect in finite nuclei.

The Pauli rearrangement effect makes the OMP shallower in a central region by 5–10 MeV, which leads to better correspondence to the depth of the phenomenological OMP.

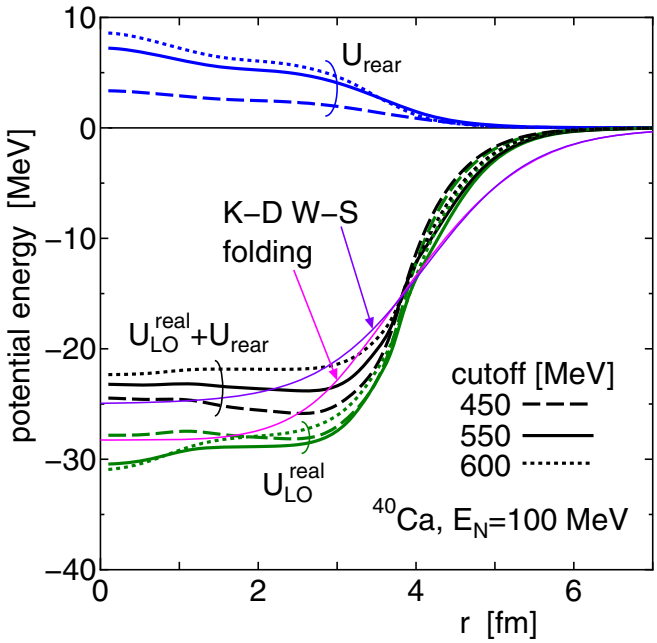

FIG. 8. Same as Fig. 7, but for $E_N = 100$ MeV.

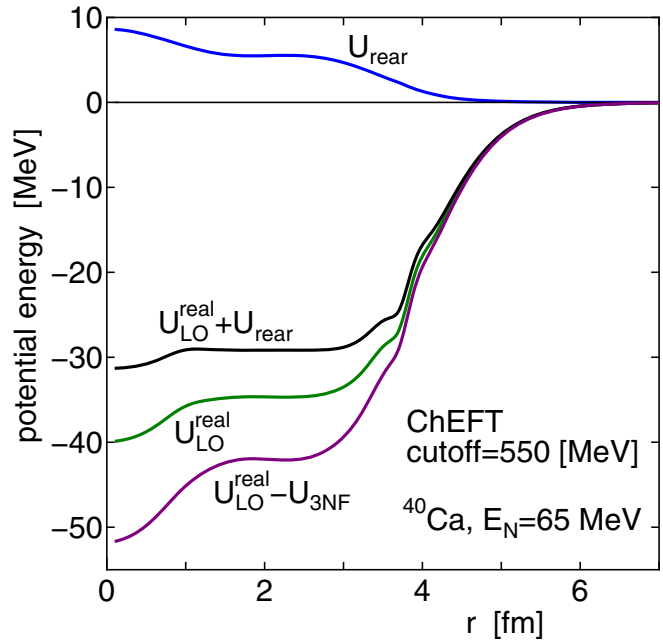

FIG. 9. The OMP in which the 3NF contribution is separated is shown for ^{40}Ca at $E_N = 65$ MeV with the cutoff scale of $\Lambda = 550$ MeV.

For comparison, the standard OMP potential in a Woods-Saxon form by Koning and Delaroche [26] is included in Figs. 7 and 8 by a thin solid curve labeled "K-D W-S". In a low-density surface area, the rearrangement effect is small.

The lowest-order s.p. potential $U_{\rm LO}^{\rm real}(p)$ contains the contribution of the 3NFs. The chief source of this repulsive contribution is understood [15] as through Pauli blocking for an excitation process of nucleon-excited states implicitly present in *NN* correlations, as is depicted in Fig. 2. It is interesting to compare the quantitative contribution of the 3NF with that of the Pauli rearrangement effect. Figure 9 shows the potential $U_{\rm LO}^{\rm real}(p) - U_{3NF}$ in which the contribution of the 3NFs is subtracted from $U_{\rm LO}^{\rm real}(p)$. The 3NF effect makes the potential shallower by about 10 MeV. The Pauli rearrangement effect provides an additional repulsive potential in a comparable magnitude. Then the resulting strength of the microscopic OMP in the inner region becomes closer to the empirical value. Two thin solid curves both in Figs. 7 and 8 indicate that if the effect of the Pauli rearrangement is incorporated, the microscopic folding potential essentially agrees with the phenomenological OMP in the whole region.

Differential cross sections and analyzing powers of proton elastic scattering on ^{40}Ca, ^{58}Ni, and ^{208}Pb at 65 MeV are evaluated in Ref. [18], using the microscopic OMP by the density-dependent effective interaction parametrized on the basis of nuclear matter G-matrix calculation with ChEFT *NN* and 3*N* interactions. The results in Fig. 3 of Ref. [18] show that the microscopic OMP explains well experimental data and the 3NF effects are small in spite of the sizable repulsive contribution in a central region as is presented in Fig. 9. This is because the nucleon elastic scattering on nuclei is governed almost by the potential in a low-density surface area. The same situation applies to the Pauli rearrangement effect. The successful description of the microscopic OMP in the literature [6–8] without the rearrangement effect is scarcely altered by the inclusion of it.

IV. CONCLUSIONS

A second-order microscopic OMP, a Pauli rearrangement potential, for a nucleon scattering state is calculated, using ChEFT *NN* and 3*N* interactions [13,14]. The second-order potential for a scattering state is real and positive. The strength of the rearrangement potential in nuclear matter is 5–10 MeV at the normal density. Because the rearrangement potential is obtained as a one-body potential, it is not straightforward to include this effect in the standard folding procedure of constructing an OMP for finite nuclei from effective two-body interactions. In this article, a simple local-density approximation is used to see qualitatively the possible contribution of the rearrangement potential in finite nuclei. It is also demonstrated that the repulsive contribution of the Pauli rearrangement effect is similar in size with the 3NF repulsive contribution.

The density dependence of the rearrangement potential indicates that the OMP becomes shallower in a central region, but is barely affected in a surface area of low density. Because the nucleon elastic scattering on nuclei is mainly determined by the peripheral region, the elastic cross section changes only slightly by the inclusion of the Pauli rearrangement effect. This explains the success of the recent microscopic OMP on the basis of realistic *NN* potentials [6–8], in spite of taking just the leading order *G*-matrix folding. However, it is meaningful to observe that the repulsive contribution improves the overall resemblance of the microscopic OMP to the empirical one.

Nucleus-nucleus scattering has also been described by the G-matrix folding prescription. In this case, higher-density regions participate in the scattering process. In previous microscopic studies of the nucleus-nucleus elastic scattering [19], the scattering cross section is still overestimated at larger angles in spite of the improvement by repulsive and absorptive effects of 3NFs. Then the additional repulsive rearrangement effect should help to further improve the description, though the actual implementation of the result in the one-body potential to the nucleus-nucleus case may not be straightforward.

ACKNOWLEDGMENTS

This work is supported by JSPS KAKENHI Grant No. JP16K17698. The author thanks M. Toyokawa for providing him numerical results of the folding potential in Figs. 7 and 8.

[1] J. P. Jeukenne, A. Lejeune, and C. Mahaux, Phys. Rev. C **10**, 1391 (1974).
[2] J. P. Jeukenne, A. Lejeune, and C. Mahaux, Phys. Rep. **25**, 83 (1976).
[3] J. P. Jeukenne, A. Lejeune, and C. Mahaux, Phys. Rev. C **16**, 80 (1977).
[4] F. A. Brieva and J. R. Rook, Nucl. Phys. A **291**, 299 (1977).
[5] F. A. Brieva and J. R. Rook, Nucl. Phys. A **291**, 317 (1977).
[6] K. Amos, P. J. Dortmans, H. V. von Geramb, S. Karataglidis, and J. Raynal, in *Advances in Nuclear Physics*, edited by J. W. Negele and E. Vogt (Plenum, New York, 2000), Vol. 25, p. 275.
[7] T. Furumoto, Y. Sakuragi, and Y. Yamamoto, Phys. Rev. C **78**, 044610 (2008).
[8] M. Toyokawa, M. Yahiro, T. Matsumoto, and M. Kohno, Prog. Theor. Exp. Phys. **2018**, 023D03 (2018).
[9] M. Lacombe, B. Loiseau, J. M. Richard, R. VinhMau, J. Conte, P. Pires, and R. deTourreil, Phys. Rev. C **21**, 861 (1980).
[10] R. Machleidt, K. Holinde, and C. Elster, Phys. Rep. **149**, 1 (1987).
[11] Th. A. Rijken, Phys. Rev. C **73**, 044007 (2006).
[12] Th. A. Rijken and Y. Yamamoto, Phys. Rev. C **73**, 044008 (2006).
[13] E. Epelbaum, W. Glöckle, and U.-G. Meißner, Nucl. Phys. A **747**, 362 (2005).
[14] E. Epelbaum, A. Nogga, W. Glöckle, H. Kamada, Ulf-G. Meißner, and H. Witala, Phys. Rev. C **66**, 064001 (2002).
[15] M. Kohno, Phys. Rev. C **88**, 064005 (2013); **96**, 059903(E) (2017).
[16] K. A. Brueckner and D. T. Goldman, Phys. Rev. **117**, 207 (1960).
[17] H. A. Bethe, Annu. Rev. Nucl. Sci. **21**, 93 (1971).
[18] M. Toyokawa, M. Yahiro, T. Matsumoto, K. Minomo, K. Ogata, and M. Kohno, Phys. Rev. C **92**, 024618 (2015); **96**, 059905(E) (2017).
[19] K. Minomo, M. Kohno, and K. Ogata, Phys. Rev. C **93**, 014607 (2016); **96**, 059906(E) (2017).
[20] J. W. Holt, N. Kaiser, G. A. Miller, and W. Weise, Phys. Rev. C **88**, 024614 (2013).
[21] R. B. Wiringa, V. G. J. Stoks, and R. Schiavilla, Phys. Rev. C **51**, 38 (1995).
[22] Th. A. Rijken, V. G. J. Stoks, and Y. Yamamoto, Phys. Rev. C **59**, 21 (1999).
[23] R. Machleidt, Phys. Rev. C **63**, 024001 (2001).
[24] J. F. Berger, M. Girod, and D. Gogny, Comput. Phys. Commun. **63**, 365 (1991).
[25] M. Toyokawa (private communication).
[26] A. J. Koning and J. P. Delaroche, Nucl. Phys. A **713**, 231 (2003).